Article

Observation of branched flow of light

https://doi.org/10.1038/s41586-020-2376-8

Received: 26 September 2019

Accepted: 16 March 2020

Published online: 1 July 2020

Check for updates

Anatoly Patsyk[1,4], Uri Sivan[1,2], Mordechai Segev[1,2]✉ & Miguel A. Bandres[3,4]✉

When waves propagate through a weak disordered potential with correlation length larger than the wavelength, they form channels (branches) of enhanced intensity that keep dividing as the waves propagate[1]. This fundamental wave phenomenon is known as branched flow. It was first observed for electrons[1–6] and for microwave cavities[7,8], and it is generally expected for waves with vastly different wavelengths, for example, branched flow has been suggested as a focusing mechanism for ocean waves[9–11], and was suggested to occur also in sound waves[12] and ultrarelativistic electrons in graphene[13]. Branched flow may act as a trigger for the formation of extreme nonlinear events[14–17] and as a channel through which energy is transmitted in a scattering medium[18]. Here we present the experimental observation of the branched flow of light. We show that, as light propagates inside a thin soap membrane, smooth thickness variations in the film act as a correlated disordered potential, focusing the light into filaments that display the features of branched flow: scaling of the distance to the first branching point and the probability distribution of the intensity. We find that, counterintuitively, despite the random variations in the medium and the linear nature of the effect, the filaments remain collimated throughout their paths. Bringing branched flow to the field of optics, with its full arsenal of tools, opens the door to the investigation of a plethora of new ideas such as branched flow in nonlinear media, in curved space or in active systems with gain. Furthermore, the labile nature of soap films leads to a regime in which the branched flow of light interacts and affects the underlying disorder through radiation pressure and gradient force.

Waves propagating through a weak disordered potential with correlation length larger than the wavelength produce surprisingly long narrow filaments (branches)[1]. Instead of producing completely random speckle patterns, the slowly varying disordered potential gives rise to focused filaments that divide to form a pattern resembling the branches of a tree. This phenomenon is called branched flow. The underlying mechanism has been traced to deflection of rays by weak correlated variations in the potential, leading to caustics[19,20]. Formally, these caustics reflect foldings of the Lagrangian manifold in phase space[21], corresponding to the concentration of rays and high field intensity along specific lines in two dimensions or over surfaces in three dimensions. Although the nature of branched flow is linear, the high field intensity may trigger additional phenomena such as nonlinear waves (such as breather and nonlinear rogue waves)[15–17]. Branched flow is now understood to be a ubiquitous wave phenomenon, but has never been observed in optics.

Here we present the experimental observation of optical branched flow. Our experiments are carried out in thin liquid soap films (Fig. 1a, b), where the weak random correlated potential arises from naturally occurring variations in film thickness[22]. We show, in experiments, that the statistical distribution of branch intensities has a heavy tail, and that the distance from the launch point to the first branching point satisfies a scaling law that depends solely on the optical potential strength and its correlation length[23].

The experimental setting for observing branched flow in liquid soap films is shown in Fig. 1a. A soap membrane consists of a thin layer of liquid stabilized by two layers of surfactant molecules (Fig. 1b and Supplementary Fig. 1). The total thickness may vary between around 5 nm ('black film') and several micrometres, with large, naturally occurring, intra-membrane thickness variations caused by the non-uniform density of surfactant molecules. These smooth thickness variations lead to variations in the effective index of refraction for light propagating within the membrane (Fig. 1c and Supplementary Fig. 3). For thick membranes, these variations in refraction index are small but when the thickness approaches one to two wavelengths, the variations become substantial and deflect light effectively.

To measure the thickness variations in the soap films directly, we construct an interference microscope in which we illuminate the thin soap film with RGB illumination (a light source with with three narrow (~25 nm) wavelength bands around red, green and blue). We observe the colourful maps shown in Fig. 1d–f, in which the colours are true colours, exactly as the light is reflected from the thin soap film. The colours indicate the local thickness of the film (see colour map in Fig. 1c). We numerically reconstruct the thickness map (see Supplementary Information), as shown in Fig. 1g–i, and find a beautiful two-dimensional landscape of hills and valleys—a disordered but correlated thickness landscape that typically varies in the 50–550-nm range. Fig. 1g–i shows examples of different thickness landscapes, each having different correlation

[1]Physics Department and Solid State Institute, Technion-Israel Institute of Technology, Haifa, Israel. [2]Russell Berrie Nanotechnology Institute, Technion-Israel Institute of Technology, Haifa, Israel. [3]CREOL, The College of Optics and Photonics, University of Central Florida, Orlando, FL, USA. [4]These authors contributed equally: Anatoly Patsyk, Miguel A. Bandres. ✉e-mail: msegev@technion.ac.il; bandres@creol.ucf.edu

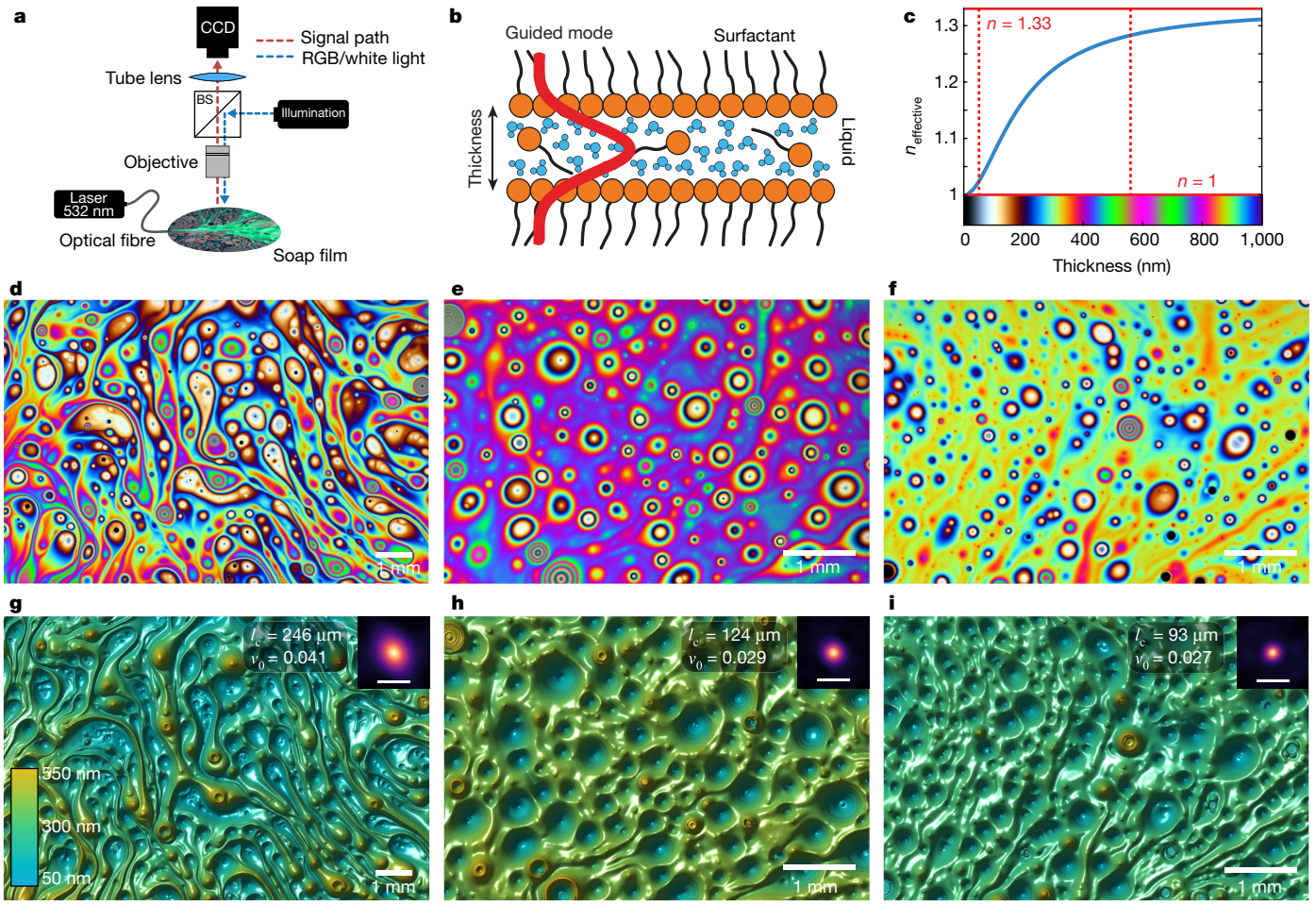

Fig. 1 | Thin liquid membranes as a platform for observing branched flow of light. a, Experimental microscope set up for observing the light propagating within a thin soap film, and the true-colour interference pattern reflected by the thin film under RGB illumination. The laser beam is coupled to the membrane by an optical fibre touching the membrane or by directly sending a collimated elliptical beam from the side of the membrane. The BS and the CCD shown in the figure refer to a beamsplitter and a charged-coupled device camera. **b**, Schematic of a thin soap film. Liquid molecules (water and/or glycerin) are held between two layers of surfactant molecules, creating a thin soap film. The film acts as a two-dimensional (slab) waveguide for the light. **c**, Effective refractive index n of the light propagating inside the film as a function of the film thickness. The red dashed lines indicate the range of thickness variation in our experiments. The colour scale shows the actual colour of the reflected RGB light at each thickness. The thickness of the membranes in the experiment is less than a micrometre. **d**–**f**, Experimental microscope images of the true-colour interference patterns created by the light reflected from the thin soap film under RGB illumination. **g**–**i**, Numerically reconstructed thickness landscape of the thin soap film from the interference colour patterns in **d**–**f**. In these three examples, the thickness variations are all in the range 50–550 nm. These thickness variations translate (through the relationship in **c**) into an effective refractive index ('potential') landscape, for the light propagating inside the thin soap film. The inset shows the autocorrelation, correlation length l_c, and strength v_0 of the effective potential. Manipulating the soap films makes it possible to produce a wide range of potential landscapes with a different l_c and v_0. The range of these parameters in our system is $v_0 \approx 1$–5% and $l_c \approx 90$–350 μm.

length and a different range of thickness variations. By manipulating the soap films—mixing or changing the surfactant/water concentration—it is possible to produce a wide range of thickness landscapes. Every membrane has a unique two-dimensional thickness landscape (a two-dimensional map). When the film is exposed to air flow in its vicinity, the thickness landscape varies over time. A membrane isolated from air movements remains stable for several minutes. The thickness landscape maps to a smooth correlated disordered effective refractive index for the light propagating within the film, through the relation in Fig. 1c. For these reasons, thin liquid films provide a perfect platform with which to observe and study the branched flow of light.

In our experimental setup, we launch a laser beam into the slab waveguide formed by a thin liquid soap film, and observe its evolution (Fig. 1a). The laser beam is coupled into the film through a single-mode fibre inserted into the film (Supplementary Fig. 2), or by coupling a broad elliptic beam (a 'plane wave' generated by a cylindrical lens) into the film. The fibre coupling is implemented by injecting the fibre into the membrane, with the fibre core aligned with the plane of the membrane slab. The fibre slightly enlarges the thickness of the membrane, but only by several micrometres in its vicinity, not affecting the rest of the membrane. The mode emitted from the fibre is much wider than the film, and hence only the first mode of the film is excited. During propagation, the beam is partially scattered from the film, which allows us to project an optical image of the light evolving in the membrane onto the camera (Fig. 1a), enabling the observation of the propagation dynamics directly in real time. As shown in Fig. 2, the beam is deflected by local random variations in the film thickness, forming focused branches that keep dividing to form a pattern that resembles the branches of a tree. The branches are created by caustics[20], which are generated when the optical wave experiences the effective refractive index landscape in the thin film. Perturbing the membrane by weak air flow in its vicinity changes the potential landscape and gives rise to different realizations of branched flow in real time, leading to the dynamic patterns shown in Supplementary Videos 1 and 2 (recorded under no illumination and

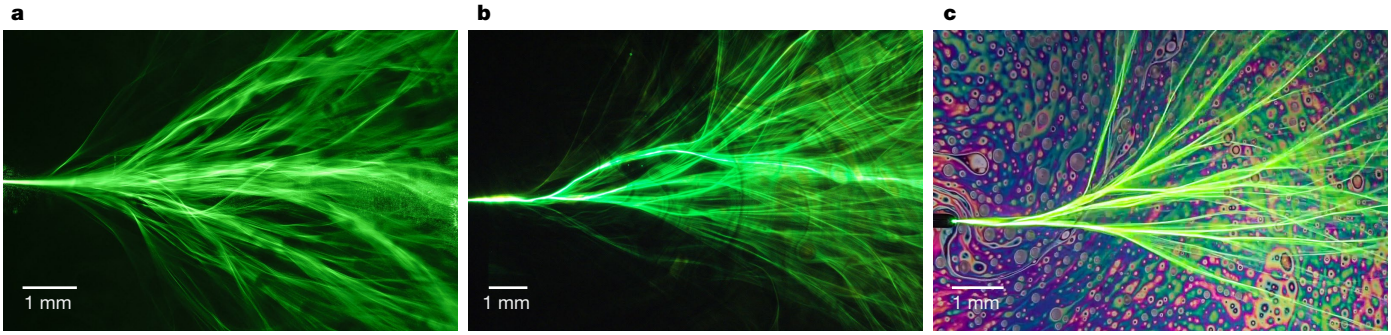

Fig. 2 | Observation of branched flow of light for an input beam generated by a single mode fibre. a, **b**, Top-view microscope images showing the evolution of a 532-nm laser beam emitted from a single mode fibre into a soap membrane. The light propagating in the film forms branched flow channelling. **c**, Branched flow pattern shown on top of the interference colour pattern generated by weak white light, making it possible to observe the potential landscape together with the branched flow.

under white light illumination using RGB sensors, respectively) for a variety of potential landscapes. By controlling the illumination intensity, we are able to observe the phenomenon of branched flow simultaneously with the underlying disordered potential landscape (Fig. 2c).

We further explore the branched flow of light under a different input beam, by launching a broad beam (approximating a plane wave) into the film and measuring its branching during propagation, as shown in Fig. 3d–f. From this figure, it is clear how the plane wave focuses at a particular distance, and how this distance varies between different landscapes of the disordered potential (Fig. 3a–c). The branched flow for a plane wave input (Fig. 3d–f) displays the expected branching of a plane wave, which was previously observed only in simulations[23–26].

Originally, branched flow was discovered in experiments with electrons travelling through a weak, smoothly varying potential in a semiconductor heterostructure, where dynamics of the electronic wavefunction was described by the time-independent Schrödinger equation

$$-\frac{\hbar^2}{2m}\nabla^2\psi + U\psi = E\psi, \tag{1}$$

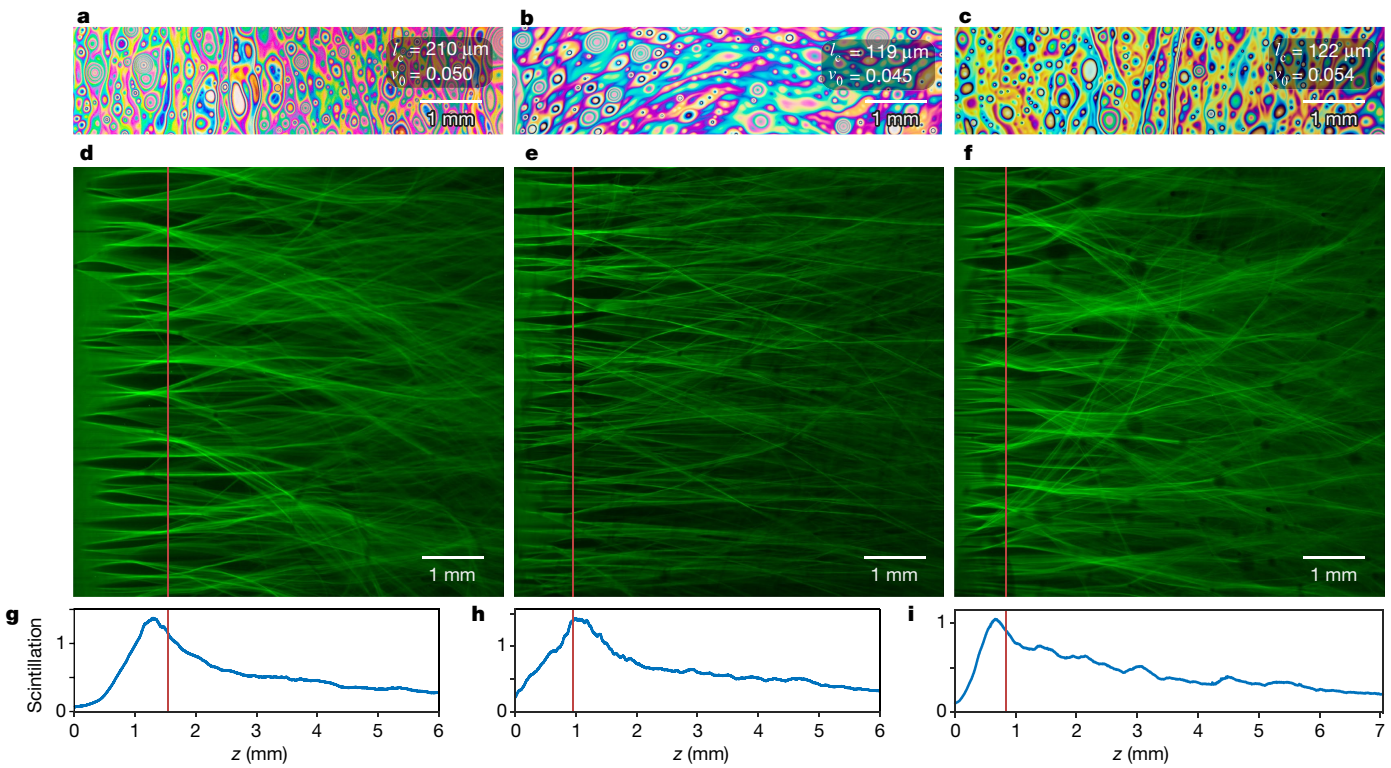

Fig. 3 | Observation of the branched flow of light for a plane wave input beam. a–**c**, Experimental microscope images of true-colour inference patterns created by the light reflected from the thin soap film under white light. The extracted values for the correlation length, l_c, and the potential strength, v_0, are given on the right. **d**–**f**, Top-view microscope images showing the amplitude (saturated at 80% of the maximum; see Supplementary Fig. 13) of the branching of a broad 532-nm laser beam as it propagates in the potential landscapes shown in **a**–**c**. **g**–**i**, Respective scintillation index, as a function of the propagation distance z, extracted from the experimental data (averaging over the transverse plane for about 10–20 realizations. The red lines in **d**–**i** mark the extracted value of $l_c v_0^{-2/3}$, which is proportional to the distance to the first branching, d_0. As shown here, we have experimentally observed that this distance, d_0, decreases as the correlation length decreases (when the potential strength is roughly the same; compare **g** and **i**). Also, d_0 decreases as the potential strength increases, (when the correlation length is roughly the same; compare **h** and **i**).

where m is the electron mass, E is the electron energy and U is the random potential in the semiconductor. In our experiments, we study the branched flow of optical waves in a slab waveguide created by a thin liquid film of thickness on the order of a single wavelength. The evolution of time-harmonic waves inside the thin film follows the Helmholtz equation

$$-\nabla^2\Psi + k_0^2(\bar{n}^2 - n_{\mathrm{eff}}^2)\Psi = k_0^2\bar{n}^2\Psi \qquad (2)$$

where $\Psi(x, z)$ is the electric field component parallel to the plane of the thin film, $k_0 = 2\pi/\lambda$ is the wavenumber in vacuum, $n_{\mathrm{eff}}(x, z)$ is the effective refractive index for a given guided mode in the waveguide and $\bar{n}^2 = \langle n_{\mathrm{eff}}^2 \rangle$ is obtained by averaging over the whole sample; see the Supplementary Information. Equations (1) and (2) are mathematically equivalent, where for the optical wave the role of energy is played by $k_0^2\bar{n}^2$, with an effective potential $V(x, z) = k_0^2(\bar{n}^2 - n_{\mathrm{eff}}^2)$ that has a zero mean $\langle V \rangle = 0$. As shown in the Supplementary Information, n_{eff} is a function of the local thickness of the slab, the optical wavelength and the refractive index of the film. In this way, local thickness variations in the film are manifested in a smoothly varying disordered potential landscape experienced by the optical wave propagating within the film.

Branched flow is universally characterized by two global parameters of the disordered correlated potential: the potential strength, which is the ratio between the standard deviation of the potential and the energy, $\upsilon_0 = \sqrt{\langle V^2 \rangle}/2E = 0.5\sqrt{\langle n_{\mathrm{eff}}^4 \rangle/\bar{n}^4 - 1}$, and the correlation length, l_c, defined by the autocorrelation function. For our two-dimensional random potential, the autocorrelation function is $c(\mathbf{r}) = \langle V(\mathbf{r})V(0) \rangle = V_0^2 f(|\mathbf{r}|/l_c)$, with $f(0) = 1$ and $V_0 = \sqrt{\langle V^2 \rangle} = \sqrt{c(0)}$. Being a universal phenomenon, branched flow is independent of the exact spatial structure of the potential and does not depend even on the form of the correlation function f, which may be any smooth function[20]. Our experimental platform of soap films allows us to generate a wide range of potential landscapes, with strengths and correlation lengths varying between $\upsilon_0 \approx 1$–5% and $l_c \approx 90$–350 μm, respectively. Typically, these statistical parameters vary only by 5% across different sections of every film (see Supplementary Fig. 6). Examples of different thickness landscapes are shown in Fig. 1g–i, which are generated in the same system under slightly different conditions (see Supplementary Information). The statistical features of branched flow are manifested in the distance from the 'source' (input beam) to the first branching point, d_0. This distance was found[8,14,20] to satisfy $d_0 \propto l_c\upsilon_0^{-2/3}$. Since our system provides for easy generation of many realizations of the random potential, we are able to study the relation between d_0 and the parameters υ_0 and l_c using large statistical ensembles, varying the correlation length, and so on. To extract d_0, we measure the scintillation index—the normalized variance of the branched flow intensity, $S(z) = \langle I^2(z) \rangle/\langle I(z) \rangle^2 - 1$, as the branches evolve along z. Here, I is the (local) intensity and the average is taken over different realizations of random potentials with the same υ_0 and l_c (ref. [8]). The scintillation index is a convenient notion, because it peaks when fluctuations are maximal, marking the onset of branching and therefore obeying the same scaling law as the distance to the first caustic[8,20].

The measured scintillation index is shown in Fig. 3g–i, for a plane wave launched into the film. To extract the scintillation index, we average the intensity in each individual realization over the transverse coordinate, which allows convergence of $S(z)$ in just a few realizations (see Supplementary Information). As shown by Fig. 3g–i, the observed scintillation index grows sharply at a distance proportional to $l_c\upsilon_0^{-2/3}$, reaches a maximum, and then declines slowly to a constant value with a long tail. As Fig. 3 shows, the position of the peak of the scintillation index is in close proximity to the calculated value of $l_c\upsilon_0^{-2/3}$ (red line in Fig. 3d–i), thus experimentally revealing the scaling law for a variety of potential landscapes. To corroborate our experiments, we also carry out simulations, shown in the Supplementary Information, of a plane wave launched into the two-dimensional refractive index landscapes of Fig. 1g–i, constructed from the actual experimental interference colour patterns of Fig. 1d–f. The correspondence between the branched flow observed directly in the experiments (Fig. 3) and the simulated branched flow using the actual measured potential landscape (Supplementary Figs. 4, 5, 8–12) is clearly visible.

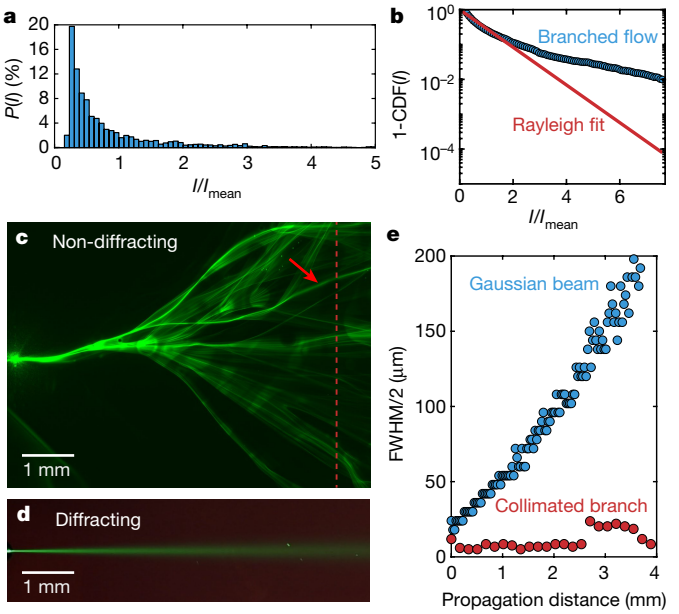

Fig. 4 | Statistical properties of experimentally observed optical branched flow for a narrow input beam. a, **b**, Probability distribution and cumulative distribution of the branches' intensities, for 100 experimental observations of branched flow, in the same film. The statistics is over the peak intensities of the branches at a fixed distance for each realization, chosen to be far enough from the input such that the branching is fully developed, as depicted in the specific realization shown in **c**, with the dashed line marking the distance from the source. As shown in **b**, the cumulative probability displays a heavy tail, as compared to that in an uncorrelated random potential (the Rayleigh fit). This implies an increased probability of finding intense waves due to the correlations in the potential landscape, as compared to an uncorrelated potential, which exhibits an exponential decay of the probability to find intense peaks. **c**, Typical experimental image of branched flow, revealing many channels where diffraction is arrested. **d**, Experimentally observed evolution of a Gaussian beam (for the same initial width as the input beam in **c**) in a flat membrane, exhibiting diffraction broadening characteristic of a homogeneous medium. **e**, Comparison between the width of the collimated branch marked by red arrow in **c** and the width of the freely diffracting Gaussian beam of **d** for a propagation interval of 4 mm.

Our experiments allow the extraction of additional statistical features of branched flow, such as the statistics of the caustic intensities. The probability density of the branched flow intensity, shown in Fig. 4a, is calculated from the imaged branched flow patterns. In this process, we measure the peak intensities, I_{peak}, along the red line in Fig. 4c, which marks a set distance from the launch point where multiple branches have already formed. We repeat this process for 100 experiments using slightly different launch positions with the same potential landscape, giving rise to 100 different branched flow patterns. We find all the intensity peaks I_{peak} at a given distance from the launch point (for example, the peaks at the plane marked by the red dashed line in Fig. 4c), identify all I_{peak} in each realization, and calculate the probability distribution (from all 100 different realizations of branched flow in the same stable membrane) shown in Fig. 4a (see details in the Supplementary Information). For a correlated potential, this statistics was predicted to display a heavy-tail distribution[9,12], whereas for a completely random potential the tail of the distribution should display exponential decay[10,14] (blue line in Fig. 4b). As exemplified by

Fig. 4b and Supplementary Fig. 7, the potential in our experiments is always correlated, and we therefore expect a considerable increase in the probability of the occurrence of localized high intensity waves. Indeed, the measured probability distribution functions displayed in Fig. 4a and b show that for low intensities, the cumulative probability follows the expected exponential decay, but that at sufficiently high intensities (above the mean intensity) the probability begins to deviate substantially from exponential decay—as the occurrence of extreme waves is increased owing to the formation of branches of high intensity by the correlated potential.

Another property of branched flow that has thus far not attracted attention is the arrest of diffraction broadening in the branches, which may be viewed as quenching of transverse diffusion. We find that the branches exhibit much less diffraction broadening than do ordinary wavepackets (beams), despite the fact that the branches are formed by scattering from random fluctuations. The branches behave as collimated narrow channels, even though the beam propagates in a random potential—in which one may expect that the beam will scatter randomly. Experimentally, it is instructive to compare the width of propagating branches from Fig. 4c to the width of the corresponding Gaussian beams propagating in a homogeneous film (Fig. 4d). Figure 4e compares the width of a characteristic branch from Fig. 4c (marked by red arrow) to the diffraction of a Gaussian beam in a film with a uniform thickness. The branched channel maintains the same width for at least ten diffraction lengths (Rayleigh lengths) before splitting again or experiencing diffraction broadening. This arrested diffraction broadening of the branches seems to be a universal feature of branched flow. Usually, nondiffracting beams are generated by nonlinear processes such as self-focusing driven by Kerr or saturable nonlinearities. Here the broadening of these wavepackets is arrested owing to scattering from the correlated random potential without nonlinear effects. Interestingly, the evolution of branched flow is fundamentally different from another phenomenon associated with random potentials: Anderson localization[27], which in the scheme of transverse localization requires the potential to be invariant in the propagation direction. Here, of course, the random variations in the potential occur anywhere in the plane, and vary in both the transverse direction and in the propagation direction. Thus, the arrest of diffraction broadening of the branches is not related to Anderson localization, despite both being generated by a random potential.

Before closing, it is important to emphasize that our experimental platform—of thin liquid films of soap—is fluidic, and so the soap film, together with the laser beam, constitutes an optofluidic system. Optofluidics, the science of light interacting with fluids, presents a host of linear and nonlinear phenomena, where light–fluid interactions give rise to effects that are fundamentally different from those encountered in light–solid interactions. The mobility of the fluid, the possibility of optically inducing deformations in the flow field, the role of diffusion and convection in transporting heat and substance, and the large-scale inhomogeneities emerging when a fluid interacts with light—all of these contribute to a variety of nonlinear phenomena that are not encountered when light interacts with solids. Examples range from nonlinearities induced by optical forces on microparticles[28], optical control of thermocapillary effects in complex nanofluids[29], particle manipulation[30] and more. In this context, using liquid soap films as a platform for experimenting with the branched flow of light has major implications for future research, such as investigating the effects of optical forces (the gradient force and radiation pressure) on branched flow. Our fluidic system may be ideal for such avenues of research, because at high enough intensities the optical forces (or heat absorption) will affect the thickness variations and perhaps create stochastic solitons. The effects of optical forces on branched flow in our thin fluidic films could offer control of flow by light and give rise to new phenomena driven by the symbiotic dynamics of the branched flow of light affecting the flow of the liquid, suggesting the occurrence of turbulence at low Reynolds numbers. Also, making the soap films slightly thicker to allow variations in the refractive index in the narrow dimension of the film, and in addition to support multiple guided modes inside the film, could give rise to branched flow in three dimensions, a phenomenon that has been proposed[31] but has thus far never been observed. In such scenarios, the full three-dimensional variation of refractive index would be required, rather than an effective refractive index.

The demonstration of the branched flow of light in our optofluidic platform of thin soap films enables access to other experimental regimes; for example, the thin soap films could be shaped into a variety of curved surfaces to study the branched flow in curved space. Supplementary Video 3 shows such an example from our experiments using a spherical shell and thus demonstrating branched flow in curved space. Such curved space experiments are intimately related to general relativity[32,33]. Moreover, when the soap film is made to be slightly absorptive, the thermal effects modify the surface tension and affect the branched flow. Likewise, if the medium displays thermal optical nonlinearity, such experiments could relate to branched flow in the Newton–Schrödinger framework of general relativity[34] in which scattering of the wavefunction has not yet been explored. Similarly, photonics offers the ability to manipulate gain and loss, and also to design parity–time-symmetric systems[35], in which branched flow has never been envisioned. Undoubtedly, the phenomenon of branched flow of light in thin liquid films suggests a plethora of ideas, and we foresee many surprising results.

Online content

Any methods, additional references, Nature Research reporting summaries, source data, extended data, supplementary information, acknowledgements, peer review information; details of author contributions and competing interests; and statements of data and code availability are available at https://doi.org/10.1038/s41586-020-2376-8.

1. Topinka, M. A. et al. Coherent branched flow in a two-dimensional electron gas. *Nature* **410**, 183–186 (2001).
2. Shaw, S. E. J. Propagation in smooth random potentials. PhD thesis, Harvard (2002); https://search.proquest.com/docview/305536276.
3. Aidala, K. E. et al. Imaging magnetic focusing of coherent electron waves. *Nat. Phys.* **3**, 464–468 (2007).
4. Jura, M. P. et al. Unexpected features of branched flow through high-mobility two-dimensional electron gases. *Nat. Phys.* **3**, 841–845 (2007).
5. Maryenko, D. et al. How branching can change the conductance of ballistic semiconductor devices. *Phys. Rev. B* **85**, 195329 (2012).
6. Liu, B. & Heller, E. J. Stability of branched flow from a quantum point contact. *Phys. Rev. Lett.* **111**, 236804 (2013).
7. Höhmann, R., Kuhl, U., Stöckmann, H.-J., Kaplan, L. & Heller, E. J. Freak waves in the linear regime: a microwave study. *Phys. Rev. Lett.* **104**, 093901 (2010).
8. Barkhofen, S., Metzger, J. J., Fleischmann, R., Kuhl, U. & Stöckmann, H.-J. Experimental observation of a fundamental length scale of waves in random media. *Phys. Rev. Lett.* **111**, 183902 (2013).
9. Heller, E. J., Kaplan, L. & Dahlen, A. Refraction of a Gaussian seaway. *J. Geophys. Res. Oceans* **113**, https://doi.org/10.1029/2008JC004748 (2008).
10. Ying, L. H., Zhuang, Z., Heller, E. J. & Kaplan, L. Linear and nonlinear rogue wave statistics in the presence of random currents. *Nonlinearity* **24**, R67 (2011).
11. Degueldre, H., Metzger, J. J., Geisel, T. & Fleischmann, R. Random focusing of tsunami waves. *Nat. Phys.* **12**, 259–262 (2016).
12. Wolfson, M. A. & Tomsovic, S. On the stability of long-range sound propagation through a structured ocean. *J. Acoust. Soc. Am.* **109**, 2693–2703 (2001).
13. Mattheakis, M., Tsironis, G. P. & Kaxiras, E. Emergence and dynamical properties of stochastic branching in the electronic flows of disordered Dirac solids. *EPL* **122**, 27003 (2018).
14. Mattheakis, M. & Tsironis, G. P. Quodons in mica. In *Extreme Waves and Branched Flows in Optical Media* 425–454 (Springer International Publishing, 2015).
15. Mattheakis, M., Pitsios, I. J., Tsironis, G. P. & Tzortzakis, S. Extreme events in complex linear and nonlinear photonic media. *Chaos Solitons Fractals* **84**, 73–80 (2016).
16. Dudley, J. M., Dias, F., Erkintalo, M. & Genty, G. Instabilities, breathers and rogue waves in optics. *Nat. Photon.* **8**, 755–764 (2014).
17. Akhmediev, N., Soto-Crespo, J. M. & Ankiewicz, A. Extreme waves that appear from nowhere: on the nature of rogue waves. *Phys. Lett. A* **373**, 2137–2145 (2009).
18. Brandstötter, A., Girschik, A., Ambichl, P. & Rotter, S. Shaping the branched flow of light through disordered media. *Proc. Natl Acad. Sci. USA* **116**, 13260–13265 (2019).
19. Berry, M. V. & Upstill, C. in *Progress in Optics. IV. Catastrophe Optics: Morphologies of Caustics and Their Diffraction Patterns* (ed. Wolf, E.) Vol. 18, 257–346 (Elsevier, 1980).

20. Kaplan, L. Statistics of branched flow in a weak correlated random potential. *Phys. Rev. Lett*. **89**, 184103 (2002).
21. Kravtsov, Y. A. & Orlov, Y. I. *Caustics, Catastrophes and Wave Fields* (Springer, 1993).
22. Patsyk, A., Bandres, M. A. & Segev, M. Interaction of light with thin liquid membranes. In *Conference on Lasers and Electro-Optics* FF3E2 (Optical Society of America, 2018); https://www.osapublishing.org/abstract.cfm?uri=CLEO_QELS-2019-FTu3D.1.
23. Metzger, J. J., Fleischmann, R. & Geisel, T. Universal statistics of branched flows. *Phys. Rev. Lett*. **105**, 020601 (2010).
24. Degueldre, H., Metzger, J. J., Schultheis, E. & Fleischmann, R. Channeling of branched flow in weakly scattering anisotropic media. *Phys. Rev. Lett*. **118**, 024301 (2017).
25. Metzger, J. J., Fleischmann, R. & Geisel, T. Statistics of extreme waves in random media. *Phys. Rev. Lett*. **112**, 203903 (2014).
26. Metzger, J. J., Fleischmann, R. & Geisel, T. Intensity fluctuations of waves in random media: what is the semiclassical limit? *Phys. Rev. Lett*. **111**, 013901 (2013).
27. Schwartz, T., Bartal, G., Fishman, S. & Segev, M. Transport and Anderson localization in disordered two-dimensional photonic lattices. *Nature* **446**, 52–55 (2007).
28. Ashkin, A., Dziedzic, J. M. & Smith, P. W. Continuous-wave self-focusing and self-trapping of light in artificial Kerr media. *Opt. Lett*. **7**, 276–278 (1982).
29. Lamhot, Y. et al. Optical control of thermocapillary effects in complex nanofluids. *Phys. Rev. Lett*. **103**, 264503 (2009).
30. Schley, R. et al. Loss-proof self-accelerating beams and their use in non-paraxial manipulation of particles' trajectories. *Nat. Commun*. **5**, 5189 (2014).
31. Heller, E. J., Fleischmann, R. & Kramer, T. Branched flow. Preprint at https://arxiv.org/abs/1910.07086 (2019).
32. Bekenstein, R., Nemirovsky, J., Kaminer, I. & Segev, M. Shape-preserving accelerating electromagnetic wave packets in curved space. *Phys. Rev. X* **4**, 011038 (2014).
33. Patsyk, A., Bandres, M. A., Bekenstein, R. & Segev, M. Observation of accelerating wave packets in curved space. *Phys. Rev. X* **8**, 011001 (2018).
34. Bekenstein, R., Schley, R., Mutzafi, M., Rotschild, C. & Segev, M. Optical simulations of gravitational effects in the Newton–Schrödinger system. *Nat. Phys*. **11**, 872–878 (2015).
35. El-Ganainy, R., Makris, K. G., Christodoulides, D. N. & Musslimani, Z. H. Theory of coupled optical PT-symmetric structures. *Opt. Lett*. **32**, 2632–2634 (2007).

Data availability

The data are available upon request.

Acknowledgements We are indebted to M. V. Berry, for suggesting to us that what we saw in the experiments is related to branched flow. This research was supported by the German-Israeli DIP project, and by the Israel Science Foundation.

Author contributions All authors contributed substantially to this work.

Competing interests The authors declare no competing interests.

Additional information

Supplementary information is available for this paper at https://doi.org/10.1038/s41586-020-2376-8.

Correspondence and requests for materials should be addressed to M.S. or M.A.B.